research papers

An experimental (120 K) and theoretical electron-density study of KMnO$_4$ and KClO$_4$

D. Marabello,^{a*} R. Bianchi,^{b} G. Gervasio^{a} and F. Cargnoni^{b}

^{a}Dipartimento di Chimica I. F. M., Via P. Giuria 7, 10125 Torino, Italy, and ^{b}CNR Istituto di Scienze e Tecnologie Molecolari, via Golgi 19, 20133 Milano, Italy. Correspondence e-mail: domenica.marabello@unito.it

The experimental electron density $\rho(\mathbf{r})$ of the two isomorphic salts KMnO$_4$ and KClO$_4$ was determined by a multipole analysis of accurate X-ray diffraction data at 120 K. The quantum theory of atoms in molecules was applied to $\rho(\mathbf{r})$ and to its Laplacian $\nabla^2\rho(\mathbf{r})$. The bonds were characterized using the topological parameters at the bond critical points of the density $\rho(\mathbf{r})$, $\nabla^2\rho(\mathbf{r})$, $G(\mathbf{r})$ (kinetic energy density), $V(\mathbf{r})$ (potential energy density) and $H(\mathbf{r})$ (total energy density). According to the classification recently proposed by Espinosa, Alkorta, Elguero & Molins [*J. Chem. Phys.* (2002), **117**, 5529–5542], the K—O and Cl—O bonds have a pure ionic and covalent character, respectively, while the Mn—O bonds show an intermediate behaviour. The results of the topological analysis of the experimental and theoretical (fully periodic Hartree–Fock and density functional calculations) electron density are in good agreement, even on a quantitative level. The atomic charges, determined by performing an integration over the topological basins, are about +2 e for Mn and Cl atoms. The ionic radius, estimated with the distance of the bond critical point from the nucleus, is in agreement with a charge of +2 e for the Mn atom.

1. Introduction

Our main interest in experimental electron-density (EED) study of transition-metal compounds is the classification of the bonding using the quantum theory of atoms in molecules (QTAM) (Bader, 1990). Previous studies on dimanganese decacarbonyl (Bianchi *et al.*, 2000) and on two polymorphic forms of a dicobalt carbonyl derivative of formula Co$_2$(CO)$_6$(μ-CO)(μ-C$_4$H$_2$O$_2$) (Bianchi *et al.*, 2001*a*,*b*) were focused on the metal atom and its binding to the surrounding ligands and on metal–metal bonding. Other authors (Abramov *et al.*, 1998; Macchi *et al.*, 1998, 1999, 2002; Macchi & Sironi 2003; Farrugia *et al.*, 2003, and references therein) have characterized bonds involving transition-metal atoms with low or zero oxidation state, while few compounds with transition metals in high oxidation states were studied (Zhurova *et al.*, 2000; Abramov *et al.*, 1995). The purpose of the present study is to investigate the EED of potassium permanganate, KMnO$_4$ (I), where manganese has its highest oxidation state. In order to make a comparison with a non-metal atom in its highest oxidation state, the isomorphic potassium perchlorate salt, KClO$_4$ (II), was also investigated. The crystal structures of (I) and (II) have been published elsewhere (Gottfried & Schusterius, 1932; Mani, 1957; Palenik, 1967) and a multipole deformation density study of (II) has appeared in the literature (Bats & Fuess, 1982). We will focus on the topological characterization of the Mn—O, Cl—O and K—O bonds. In order to better understand the nature of such

interactions, the experimental topological analysis will be compared with the theoretical one in the solid state.

2. Experimental section

2.1. Data collection and reduction

For both salts, a crystal suitable for data collection was obtained from water solution and was cooled to 120 K within nearly 5 h. The intensity data were collected with graphite-monochromated Mo $K\alpha$ radiation (λ = 0.71073 Å) on a Siemens-P4 diffractometer equipped with a Bruker APEX CCD detector and an N$_2$ gas-stream low-temperature device. The data used in the refinement process were obtained using the following programs: Bruker AXS *SMART* (collection), *SAINT* (integration) and *SADABS* (absorption correction), *SHELXTL* (molecular graphics) (Sheldrick, 1998). The reflections were collected with the φ-scan technique ($\Delta\varphi$ = 0.3°) and, due to the good quality of the crystals, exposure time of the frames was only 10 s for the low-2θ data and 20 s for the high-2θ data.

2.2. Refinements

For refinements, the *VALRAY* software (Stewart & Spackman, 1983) interfaced by one of us (RB) with the *TOPOND98* (Gatti & Bianchi, 1996; Gatti, 1999) program was used throughout.

Table 1
Crystal data and refinement parameters for $KMnO_4$ and $KClO_4$.

	$KMnO_4$	$KClO_4$
Crystal data		
Empirical formula	$KMnO_4$	$KClO_4$
Formula weight (a.m.u.)	158.04	138.55
Crystal dimensions (mm)	$0.17 \times 0.22 \times 0.28$	$0.22 \times 0.30 \times 0.34$
Lattice type,	Orthorhombic,	Orthorhombic,
space group	$Pnma$	$Pnma$
Unit-cell dimensions (Å)	$a = 9.0509\ (7)$	$a = 8.7684\ (3)$
	$b = 5.6381\ (4)$	$b = 5.6237\ (2)$
	$c = 7.3582\ (5)$	$c = 7.2039\ (3)$
Volume (Å^3)	375.49 (5)	355.23 (2)
Z (No. of molecules in unit cell)	4	4
Measurement temperature (K)	120	126
Density (calculated) (g cm^{-3})	2.796	2.591
$F(000)$	304	272
Absorption coefficient (mm^{-1})	4.474	2.092
Reflections collected	18417	15985
Unique reflections	1791	1604
R_{int}	0.0317	0.0253
(R_{int} before SADABS)	(0.0610)	(0.0532)
R_σ	0.0159	0.0127
h,k,l limits	$-11 \leq h \leq 11$	$-17 \leq h \leq 17$
	$-15 \leq k \leq 15$	$-9 \leq k \leq 11$
	$-18 \leq l \leq 18$	$-14 \leq l \leq 12$
θ min. / max. (°)	3.57 / 46.76	3.66 / 45.61
μ (Mo $K\alpha$) mm^{-1}	4.474	2.092
Min./max. transmission coefficient	0.833	0.865
Multipole refinement results		
N_o (No. of reflections)	1791	1604
Refinement method	POP	POP
N_p (No. of parameters)	97	92
$R(F)$	0.0194	0.0161
$wR(F)$	0.0179	0.0149
$R(F^2)$	0.0194	0.0203
$wR(F^2)$	0.0313	0.0267
S	0.943	1.020
k (scale factor)	1.030 (5)	0.985 (4)
(Shift/s.u.)$_{max}$	<0.01	<0.01

$R_{int} = \sum ||F_o|^2 - |F_o|^2 (\text{mean})| / \sum |F_o|^2$; $R_\sigma = \sum [\sigma |F_o|^2] / \sum [|F_o|^2]$;
$R(F) = \sum ||F_o| - k|F_c|| / \sum |F_o|$; $wR(F) = [\sum w(|F_o| - k|F_c|)^2 / \sum w|F_o|^2]^{1/2}$;
$R(F^2) = \sum ||F_o|^2 - k^2|F_c|^2| / \sum |F_o|^2$; $wR(F^2) = [\sum w(|F_o|^2 - k^2|F_c|^2)^2 / \sum w|F_o|^4]^{1/2}$;
$S = [\sum w(|F_o|^2 - k^2|F_c|^2)^2 / (N_o - N_p)]^{1/2}$.

For both compounds, independent-atom model (IAM) refinements of the scale factor, of the extinction parameter, and of positional and anisotropic displacement parameters were carried out. Atomic scattering factors including those for anomalous scattering of the K, Mn, Cl and O atoms were taken from *International Tables for Crystallography* (1995, Vol. C). The quantity minimized was $\sum w(|F_o|^2 - k^2|F_c|^2)^2$ based on all independent reflections and weights $w = 1/\sigma^2(F_o^2)$.

The atomic parameters from the conventional refinements were used as starting values for further multipole refinements by the aspherical-atom formalism developed by Stewart (1976). The density at each rigid pseudoatom was approximated using the following multipole model (POP):

$$\rho_{\text{atomic}}(\mathbf{r}) = P_{\text{core}}\rho_{\text{core}}(r) + P_{\text{valence}}\rho_{\text{valence}}(r)$$
$$+ \sum_{l=1}^{l_{max}} R_l(r) \sum_{m=-l}^{l} P_{lm} Y_{lm}(\theta, \varphi),$$

where ρ_{core} and ρ_{valence} are the spherical core and valence densities, respectively, and the summation in the third term accounts for the valence deformations. Only for the Mn atom was ρ_{core} divided into two components: $P_{\text{core}}\rho_{\text{core}}(r) = P_{\text{core1}}\rho_{\text{core1}}(r) + P_{\text{core2}}\rho_{\text{core2}}(r)$.

For all atoms, the core and valence densities were calculated from Hartree–Fock atomic wavefunctions (Clementi & Roetti, 1974). $R_l(r)$ is a radial function of Slater type or a fixed linear combination of exponentials, and $Y_{lm}(\theta,\varphi)$ is a real spherical harmonic. P_{core}, P_{valence} and P_{lm} are parameters to optimize. On the Mn-atom position, functional expansions up to the hexadecapole level were introduced ($l_{max} = 4$), whereas the expansions were terminated at the octupole level at the K-, Cl- and O-atom positions. A single P_{core} parameter was refined for the O atoms and P_{core} of the K atom was constrained to be equal to P_{core1} of the Mn atom. For the higher multipoles ($l \geq 1$), the Slater-type exponents, α's, were assigned fixed values based on theory (Hehre *et al.*, 1970; Pietro & Hehre, 1983). The unit-cell electron-neutrality condition was imposed during the multipole refinement. The data were corrected for isotropic extinction as determined by least-squares refinement ($y_{min} = 0.941$ and 0.846 for (I) and (II), respectively, $y = |F_o|/|F_{\text{corr}}|$). To test the effect of the anharmonicity in the thermal motion, we introduced a third-order Gram–Charlier (Johnson & Levy, 1974) coefficient in the least-squares procedures for (I) and (II). Introduction of anharmonic parameters led to no significant improvement in the multipole analyses, so they were excluded from the final models. The Hirshfeld rigid-bond test (Hirshfeld, 1976) was applied to the final thermal parameters. The r.m.s. differences of the mean-square displacement amplitudes for bonded atoms along the bond vector in (I) and (II) were less than 0.001 Å; therefore, the final models are consistent with the rigid-bond hypothesis.

Crystal data and refinement parameters are listed in Table 1.

2.3. Theoretical calculations

The wavefunctions of crystals (I) and (II) have been determined by means of all-electrons first principles fully periodic computations. To compare data obtained with different theoretical schemes, we adopted either the restricted Hartree–Fock (RHF) or the density-functional-theory (DFT) approach, implemented in the *CRYSTAL98* (Saunders *et al.*, 1999) package within the LCAO (linear combination of atomic orbitals) formalism. In the case of DFT computations, we selected the Becke and LYP potentials for the exchange and correlation part of the pseudo-Hamiltonian, respectively. For both (I) and (II), the X-ray experimental cell parameters and atomic coordinates were adopted. As concerns the basis-set choice, computations were carried out with a slightly modified 3-21G set. In the case of non-metallic atoms (Cl and O), the 3-21G basis was retained as such, while, for metals (K and Mn), the outermost shells were modified, because they contain very diffuse Gaussian functions that lead to linear dependence in the computations. For K and Mn, the outermost sp shell was eliminated and the contraction of the inner

Table 2
Atomic fractional coordinates and anisotropic thermal parameters ($\mathring{A}^2 \times 10^2$) from the multipole refinement.

The temperature factor is given by $\exp[-2\pi^2(U_{11}h^2a^{*2} + \ldots + 2U_{23}klb^*c^*)]$.

KMnO₄

Atom	x	y	z	U_{11}	U_{12}	U_{13}	U_{22}	U_{23}	U_{33}
K	0.31877 (2)	0.25000	0.65798 (2)	1.121 (6)	0.000	−0.015 (4)	2.346 (9)	0.000	1.366 (7)
Mn	0.43748 (1)	0.25000	0.19264 (2)	1.008 (4)	0.000	0.009 (3)	1.238 (5)	0.000	0.980 (4)
O(1)	0.3107 (2)	0.25000	0.0385 (2)	2.54 (5)	0.000	−1.10 (4)	2.77 (6)	0.000	1.59 (4)
O(2)	0.5998 (2)	0.25000	0.1022 (3)	1.74 (5)	0.000	1.24 (4)	3.650 (7)	0.000	2.89 (6)
O(3)	0.41857 (9)	0.0164 (1)	0.3186 (1)	1.91 (3)	−0.04 (2)	−0.18 (2)	1.33 (3)	0.50 (2)	1.96 (3)

KClO₄

Atom	x	y	z	U_{11}	U_{12}	U_{13}	U_{22}	U_{23}	U_{33}
K	0.31965 (1)	0.25000	0.66139 (2)	1.024 (3)	0.000	0.033 (3)	1.461 (5)	0.000	1.239 (4)
Cl	0.43049 (2)	0.25000	0.18838 (3)	0.852 (4)	0.000	0.012 (3)	0.966 (6)	0.000	0.890 (5)
O(1)	0.3060 (1)	0.25000	0.0571 (1)	1.27 (2)	0.000	−0.82 (2)	2.41 (4)	0.000	2.07 (3)
O(2)	0.5746 (1)	0.25000	0.0939 (2)	1.52 (2)	0.000	−0.57 (2)	1.80 (3)	0.000	1.25 (3)
O(3)	0.41911 (7)	0.0406 (1)	0.3056 (1)	1.59 (2)	0.01 (1)	0.12 (1)	1.12 (2)	−0.36 (1)	1.44 (2)

one was released. To evaluate the dependence of our theoretical results on the quality of the basis set, we carried out computations with the larger 6-31G basis set, modified according to the criterion adopted for the 3-21G one. In the case of the KMnO₄ crystal only, serious problems were encountered to obtain a well converged wavefunction, whatever theoretical approach was adopted. These problems probably are connected to the poorness of single determinant wavefunctions in the description of transition-metal atoms. On the contrary, for KClO₄ the topological analysis of the electron density evidenced no significant differences between the 3-21G and 6-31G basis sets. Thus, we are confident that, even at the 3-21G level, theoretical data can be properly compared with experimental ones for both salts. To perform the QTAM analysis of the analysed compound, the *TOPOND98* code

(Gatti, 1999) interfaced with *CRYSTAL98* was used. Only DFT results are reported because they are very similar to the RHF ones.

Further details of the crystal structure investigations can be obtained from the Fachinformationszentrum Karlsruhe, 76344 Eggenstein-Leopoldshafen, Germany [fax: (+49) 7247 808 666; e-mail: infodienste@fiz.karlsruhe.de] quoting the depository numbers CSD-413443 (KMnO₄) and CSD-413444 (KClO₄). Multipole population parameters are reported in supplementary materials.[1]
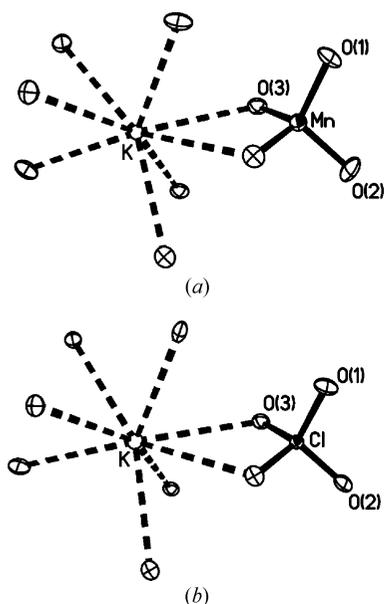
3. Results and discussion

3.1. Structural properties

The coordination polyhedra of O atoms around the K atom and around the Mn or Cl atoms are illustrated in Fig. 1 and the atomic fractional coordinates with anisotropic thermal parameters are listed in Table 2.

Four O atoms are tetrahedrally coordinated around the Mn or Cl atom and the two average Mn—O and Cl—O distances [1.615 (1) and 1.444 (1) Å, respectively] are remarkably different. The K ion is coordinated to eight O atoms: two of them belong to the same (Mn or Cl)O₄ moiety and the others to six different (Mn or Cl)O₄ groups. The geometry of the octacoordination corresponds to an irregular cubic antiprism. The K-ion coordination polyhedra are similar in the two salts; in particular, the average K—O bond distances are 2.843 (3) and 2.863 (2) Å for (I) and (II), respectively. The O(3) atom has a tetrahedral coordination (three K atoms and one Mn or Cl atom) while O(1) and O(2) have a quite distorted tetrahedral environment.

Figure 1
ORTEP plot (50% probability) of coordination polyhedra of (I) (*a*) and (II) (*b*).

[1] Supplementary data, including CIFs, structure factors and multipole population parameters, are available from the IUCr electronic archives (Reference: XC5001). Services for accessing these data are described at the back of the journal.
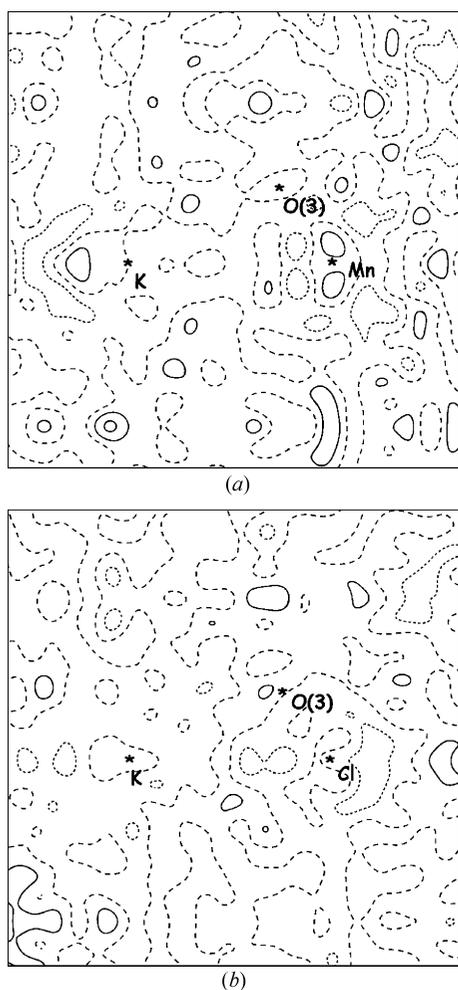
3.2. Difference electron densities

The residual maps (Figs. 2a,b) based on $F_{observed} - F_{multipole}$ in the plane defined by K, Mn (or Cl) and O(3) atoms show no significant features and the largest peaks are 0.22 (5) and 0.19 (5) e Å^{-3} for (I) and (II), respectively. For both salts, the average standard deviation (σ) of the total density, representative of the error in the difference density, is 0.08 e Å^{-3} at positions away from the nuclei. All the features in the residual maps are below 3σ, indicating that the POP models used in the refinements are adequate.
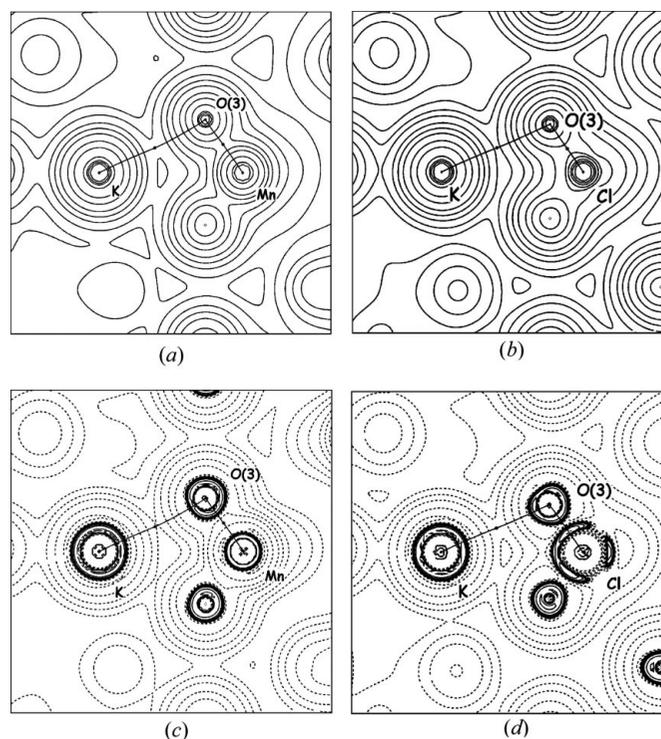
3.3. Topology of electron density, energy descriptors and bond classification

The QTAM (Bader, 1990) is a useful tool to correlate the bonding properties with the topology of the electron density $\rho(\mathbf{r})$ and of its Laplacian $\nabla^2\rho(\mathbf{r})$. Two atoms are to be considered bonded when a bond path (a line of maximum density) connects the two nuclei and there is a $(3, -1)$ critical point or bond critical point (BCP) on this bond path at $\mathbf{r}_c$. The Laplacian $\nabla^2\rho(\mathbf{r})$ is defined as the sum of the three eigenvalues

of the density Hessian matrix. In this paper, interatomic bonds are classified in 'shared' and 'closed-shell' interactions, depending on the sign of $\nabla^2\rho(\mathbf{r}_c)$ $[\nabla^2\rho(\mathbf{r}_c) < 0$ and > 0, respectively]. Further information about the bond properties can be obtained from the energy density values $[G(\mathbf{r}_c) = $ kinetic energy density; $V(\mathbf{r}_c) = $ potential energy density; $H(\mathbf{r}_c) = G(\mathbf{r}_c) + V(\mathbf{r}_c) = $ total energy density], estimated in the case of the EED from the $\rho(\mathbf{r}_c)$ and $\nabla^2\rho(\mathbf{r}_c)$ values, using the formulae proposed by Abramov (1997) and Espinosa et al. (1998). For the 'closed-shell' interactions, the Abramov estimate of $G(\mathbf{r}_c)$ is within 4% of the high-quality Hartree–Fock values for kinetic energy densities at bond critical points, whereas for 'shared' type the estimate is only in semi-quantitative agreement with the theoretical values. Recently, Espinosa et al. (2002) proposed a classification of the atomic interactions dividing them into three characteristic states: pure closed shell [CS, region I, $\nabla^2\rho(\mathbf{r}_c) > 0$, $H(\mathbf{r}_c) > 0$], pure shared shell [SS, region III, $\nabla^2\rho(\mathbf{r}_c) < 0$, $H(\mathbf{r}_c) < 0$] and transit closed shell [CS, region II, $\nabla^2\rho(\mathbf{r}_c) > 0$, $H(\mathbf{r}_c) < 0$]. This classification was advanced using the topological and energetic properties of the theoretical $\rho(\mathbf{r})$ of the isolated $H\cdots F$ system and of 79 neutral, positively and negatively charged $X-H\cdots F-Y$ complexes. The boundaries among regions I, II, and III are defined by $H(\mathbf{r}_c) = 0$ $[i.e. |V(\mathbf{r}_c)|/G(\mathbf{r}_c) = 1]$ and by $\nabla^2\rho(\mathbf{r}_c) = 0$ $[i.e. |V(\mathbf{r}_c)|/G(\mathbf{r}_c) = 2]$. Inside region I (pure CS), the bond

Figure 2
Residual density maps for (I) (a) and (II) (b), on the planes defined by K, Mn or Cl and O(3) atoms. Solid lines represent positive contours, short dashed lines represent negative contours, and the wide dashed lines represent the zero contour. The contour interval is 0.10 e Å^{-3}.

Figure 3
Experimental $\rho(\mathbf{r})$ maps for (I) (a) and (II) (b), on the planes defined by K, Mn or Cl and O(3) atoms. The corresponding maps of $\nabla^2\rho(\mathbf{r})$ are reported in (c) and (d). The absolute values of the contours (a.u.) increase from the outermost one inwards in steps of 2×10^n, 4×10^n and 8×10^n, with n beginning at -3 and increasing in steps of 1. For $\nabla^2\rho(\mathbf{r})$ maps, positive values are denoted by dashed contours, negative values are denoted by solid contours. The two trajectories (bond paths) of $\rho(\mathbf{r})$ that originate at the BCP are superimposed on the maps.

D. Marabello et al. · Electron-density study of KMnO$_4$ and KClO$_4$

Table 3
Bond critical point properties for (I).

R = distance (Å) between atoms X and Y; R_x = distance between the nucleus of atom X and the bond critical point. First row from POP model, second row from DFT calculations.

$X-Y$	R (Å)	R_x (Å)	$\rho(\mathbf{r}_c)$ (e Å^{-3})	$\nabla^2\rho(\mathbf{r}_c)$ (e Å^{-5})	λ_1 (e Å^{-5})	λ_2 (e Å^{-5})	λ_3 (e Å^{-5})	$G(\mathbf{r}_c)$ (Hartree Å^{-3})	$V(\mathbf{r}_c)$ (Hartree Å^{-3})	$|V(\mathbf{r}_c)|/G(\mathbf{r}_c)$	$H(\mathbf{r}_c)$ (Hartree Å^{-3})	$H(\mathbf{r}_c)/\rho(\mathbf{r}_c)$ (Hartree e^{-1})
K—O(3)	2.9643 (8)	1.520	0.057 (2)	0.98 (2)	−0.15	−0.12	1.25	0.05	−0.04	0.80	0.01	0.18
		1.496	0.056	1.35	−0.21	−0.19	1.75	0.07	−0.06	0.74	0.02	0.35
K—O(1)^{i}	2.801 (1)	1.457	0.084 (5)	1.56 (2)	−0.29	−0.29	2.14	0.09	−0.06	0.67	0.03	0.35
		1.425	0.084	1.83	−0.32	−0.32	2.47	0.11	−0.09	0.83	0.02	0.22
K—O(3)^{ii}	2.8173 (8)	1.484	0.070 (2)	1.26 (1)	−0.21	−0.18	1.65	0.07	−0.05	0.71	0.02	0.28
		1.428	0.082	1.82	−0.32	−0.31	2.45	0.11	−0.09	0.82	0.02	0.23
K—O(3)^{iii}	2.8753 (8)	1.462	0.082 (2)	1.48 (2)	−0.26	−0.26	2.00	0.08	−0.06	0.75	0.02	0.24
		1.455	0.071	1.62	−0.27	−0.26	2.15	0.09	−0.07	0.79	0.02	0.28
K—O(2)^{iv}	2.755 (2)	1.429	0.092 (5)	1.74 (3)	−0.33	−0.32	2.39	0.10	−0.07	0.70	0.03	0.33
		1.409	0.092	1.99	−0.36	−0.36	2.71	0.12	−0.10	0.85	0.02	0.20
Mn—O(1)	1.613 (1)	0.850	1.67 (4)	27 (1)	−13	−12	52	3.15	−4.41	1.40	−1.26	−0.75
		0.838	1.57	25	−10	−10	45	2.49	−3.24	1.30	−0.74	−0.47
Mn—O(2)	1.613 (2)	0.849	1.66 (4)	28 (1)	−13	−12	53	3.18	−4.40	1.38	−1.22	−0.73
		0.838	1.57	25	−10	−10	45	2.50	−3.24	1.30	−0.74	−0.47
Mn—O(3)	1.6195 (8)	0.854	1.62 (3)	28 (1)	−12	−12	52	3.10	−4.25	1.37	−1.15	−0.71
		0.841	1.55	24	−10	−10	44	2.43	−3.17	1.30	−0.73	−0.47

Symmetry operations: (i): $x, y, z + 1$; (ii): $-x + 1, -y, -z + 1$; (iii): $-x + 0.5, -y, z + 0.5$; (iv): $x - 0.5, y, -z + 0.5$.

Table 4
Bond critical point properties for (II).

R = distance (Å) between atoms X and Y; R_x = distance between the nucleus of atom X and the bond critical point. First row from POP model, second row from DFT calculations.

$X-Y$	R (Å)	R_x (Å)	$\rho(\mathbf{r}_c)$ (e Å^{-3})	$\nabla^2\rho(\mathbf{r}_c)$ (e Å^{-5})	λ_1 (e Å^{-5})	λ_2 (e Å^{-5})	λ_3 (e Å^{-5})	$G(\mathbf{r}_c)$ (Hartree Å^{-3})	$V(\mathbf{r}_c)$ (Hartree Å^{-3})	$|V(\mathbf{r}_c)|/G(\mathbf{r}_c)$	$H(\mathbf{r}_c)$ (Hartree Å^{-3})	$H(\mathbf{r}_c)/\rho(\mathbf{r}_c)$ (Hartree e^{-1})
K—O(3)	2.9525 (7)	1.507	0.049 (2)	1.07 (1)	−0.16	−0.14	1.37	0.06	−0.04	0.67	0.02	0.41
		1.479	0.062	1.46	−0.23	−0.22	1.91	0.08	−0.06	0.75	0.02	0.34
K—O(1)^{i}	2.853 (1)	1.468	0.064 (3)	1.36 (2)	−0.25	−0.22	1.83	0.07	−0.05	0.71	0.02	0.31
		1.447	0.074	1.69	−0.29	−0.28	2.26	0.10	−0.08	0.80	0.02	0.27
K—O(3)^{ii}	2.8239 (6)	1.474	0.079 (2)	1.50 (2)	−0.31	−0.28	2.09	0.08	−0.06	0.75	0.02	0.25
		1.425	0.084	1.86	−0.33	−0.32	2.51	0.11	−0.09	0.82	0.02	0.24
K—O(3)^{iii}	2.8518 (6)	1.471	0.069 (2)	1.41 (1)	−0.26	−0.23	1.90	0.08	−0.05	0.63	0.03	0.43
		1.434	0.079	1.79	−0.31	−0.30	2.40	0.10	−0.08	0.80	0.02	0.26
K—O(2)^{iv}	2.829 (1)	1.473	0.066 (3)	1.35 (2)	−0.23	−0.23	1.81	0.07	−0.05	0.71	0.02	0.30
		1.460	0.069	1.61	−0.26	−0.25	2.12	0.09	−0.08	0.80	0.02	0.28
Cl—O(1)	1.4445 (9)	0.699	2.44 (3)	−7.6 (6)	−17.0	−17.0	26.4	3.2	−7.0	2.19	−3.8	−1.56
		0.698	2.10	−6.7	−12.6	−12.6	18.4	1.6	−3.6	2.30	−2.1	−0.98
Cl—O(2)	1.435 (1)	0.689	2.54 (3)	−8.5 (6)	−18.5	−17.4	27.4	3.4	−7.4	2.18	−4.0	−1.57
		0.687	2.14	−8.4	−12.7	−12.7	17.0	1.6	−3.8	2.36	−2.2	−1.03
Cl—O(3)	1.4524 (7)	0.702	2.44 (3)	−7.6 (6)	−17.6	−16.6	26.6	3.2	−6.9	2.16	−3.7	−1.51
		0.707	2.07	−5.6	−12.5	−12.5	19.4	1.6	−3.4	2.21	−1.9	−0.91

Symmetry operations: (i): $x, y, z + 1$; (ii): $-x + 1, -y, -z + 1$; (iii): $-x + 0.5, -y, z + 0.5$; (iv): $x - 0.5, y, -z + 0.5$.

degree parameter [BD = $H(\mathbf{r}_c)/\rho(\mathbf{r}_c)$] is an index of no covalent interaction and is indicated as a softening degree (SD) per electron-density unit at the BCP; the weaker the interaction, the greater the SD magnitude. In regions II and III, the BD parameter measures the covalence degree (CD) of the pairwise interaction; the stronger the interaction, the greater the CD magnitude. Although the BD parameter was tested on hydrogen-bonded systems, it has been defined to classify any bonding interaction on a continuous scale (Espinosa *et al.*, 2002) and we applied it to our compounds (see below). In Fig. 3 are reported EED and Laplacian maps for (I) and (II) on the plane containing K, Mn (or Cl) and O(3) atoms. We list in Tables 3 and 4 the BCP properties of the two salts.

All the expected bond paths were found. The K—O bonds in both salts show the same features, *i.e.* positive values of $\nabla^2\rho(\mathbf{r}_c)$, low values of $\rho(\mathbf{r}_c)$ and $H(\mathbf{r}_c)$ slightly positive but very near to zero; these features are typical of ionic interactions and, following the classification of Espinosa *et al.* (2002), they are pure closed-shell (CS) bonds. The topological parameters of K—O bonds at $\mathbf{r}_c$ for the IAM model and POP model are quite similar (see Tables 2 and 3), in agreement with their ionic character. The Mn—O bonds show values of $\rho(\mathbf{r}_c)$ and $\nabla^2\rho(\mathbf{r}_c)$ greater than K—O bonds and negative values of $H(\mathbf{r}_c)$; these interactions can be associated with the transit closed-shell (CS) type. Similar topological values were obtained by Tsirelson *et al.* (1998) for the Ta—O bonds in the EED work on
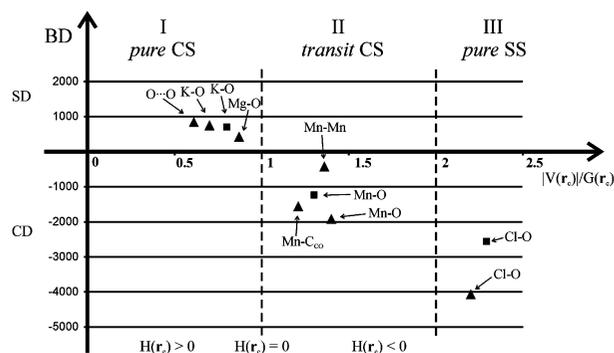
the $KTaO_3$ salt (Zhurova *et al.*, 2000). The Cl—O bonds show large values of $\rho(\mathbf{r}_c)$ and largely negative values of $\nabla^2\rho(\mathbf{r}_c)$ and $H(\mathbf{r}_c)$; this behaviour is typical of covalent interactions and they can be classified as pure shared-shell (S) interactions.

A good agreement between the theoretical and experimental topological and energetic parameters at the BCPs, reported in Tables 3 and 4, is observed. For the energetic descriptors of Mn—O and Cl—O bonds, the agreement is only qualitative, except for the ratio $|V(\mathbf{r}_c)|/G(\mathbf{r}_c)$, where the agreement is satisfactory. Our experimental values of $|V(\mathbf{r}_c)|/G(\mathbf{r}_c)$ and of BD for Cl—O bonds are in fine agreement with the corresponding ones reported in a previous investigation of ClO_4^- groups (Lee *et al.*, 2002).

The topological descriptors of bonds involving transition metals reported in the literature indicate that these kinds of interactions belong to the transit region II. In Fig. 4 is shown the trend of the experimental and theoretical bond degree parameters as a function of $|V(\mathbf{r}_c)|/G(\mathbf{r}_c)$ for (I) and (II). For the sake of comparison, the BD parameters of the Mn—Mn and the Mn—C_{CO} interactions (Bianchi *et al.*, 2000), of the ionic bond Mg—O (Tsirelson *et al.*, 1998) and of the van der Waals interaction O···O (Bianchi *et al.*, 2001*a,b*), are also reported.

The Mg—O, K—O and O···O interactions are associated with region I (pure CS type). The SD values indicate a weakening of the bonds moving from Mg—O to O···O interactions. The Mn—O, Mn—Mn and Mn—C_{CO} bonds lie in the intermediate region II (transit CS type). Finally, the Cl—O bond lies in region III (pure SS type). This bond classification is in keeping with that reported in the topological study of $Mn_2(CO)_{10}$ (Bianchi *et al.*, 2000). For the interactions with $H(\mathbf{r}_c) < 0$ (regions II and III), the magnitude of the experimental CD parameter grows from Mn—Mn to Cl—O bonds (for metal–metal bonds, see Gervasio *et al.*, 2004).

Tsirelson (1999) observed also that ionic bonds are characterized by $0.07 < \rho(\mathbf{r}_c) < 0.25$ e Å^{-3} and $0.12 < |\lambda_1|/\lambda_3 < 0.17$. Also in the case of the (I) and (II) salts the $\rho(\mathbf{r}_c)$ and $|\lambda_1|/\lambda_3$ values for K—O bonds fall within the above ranges [$\rho(\mathbf{r}_c) = 0.077$ e Å^{-3} average; $|\lambda_1|/\lambda_3 = 0.13$ average]. On the contrary, we have $\rho(\mathbf{r}_c) = 1.65$ e Å^{-3} average, $|\lambda_1|/\lambda_3 = 0.24$ e Å^{-5}

average and $\rho(\mathbf{r}_c) = 2.47$ e Å^{-3} average, $|\lambda_1|/\lambda_3 = 0.66$ e Å^{-5} average for Mn—O and Cl—O bonds, respectively.

3.4. Topology of the Laplacian of electron density

The critical points of $-\nabla^2\rho(\mathbf{r})$ can be classified by the pair (ω,σ), where ω is the number of non-zero eigenvalues of the Hessian matrix associated with $\nabla^2\rho(\mathbf{r})$ and σ is the number of positive eigenvalues minus the number of negative ones. The experimental maps of $\nabla^2\rho(\mathbf{r})$ show large differences between the regions around the Mn and Cl nuclei (see Figs. 3*c, d*), while the regions of $\nabla^2\rho(\mathbf{r})$ around the K atoms are similar in the two compounds. The valence shell charge concentration (VSCC) of K atoms does not exhibit $(3,-3)$ critical points, at either experimental or theoretical level, and therefore K atoms may be considered essentially spherical. The experimental VSCC's of Mn and Cl atoms show four $(3,-3)$ critical points facing the neighbouring O atoms. These data are in agreement with the theoretical ones for the Cl atom, while we found some discrepancies in the case of the Mn atom. At the restricted Hartree–Fock level, the VSCC of Mn has four $(3,-3)$ critical points facing the O atoms, and four $(3,-3)$ in non-bonding regions. Conversely, at density functional level, the Mn atoms have no $(3,-3)$ critical points along the Mn—O bonds, but they have four $(3,-3)$ in regions between the Mn—O bonds. These features are due to small differences in the electron-density distribution around the Mn atom, and probably reflect the difficulty in describing properly half-filled d shells and their polarization in the theoretical computations.

The estimated average VSCC radii taken from the experiment are 0.75 Å for Cl, 0.42 Å for Mn, 0.65 Å for K and 0.48 Å for O atoms. Similar values for Mn and O atoms were found in the complex $Mn_2(CO)_{10}$ (Bianchi *et al.*, 2003) despite the different formal oxidation state and charge of the Mn atom.

3.5. Atomic charges and ionic radii

The atomic charges for both compounds were determined by performing an integration over the topological atomic basins Ω (Bader, 1990) in $\rho(\mathbf{r})$. A summation of the atomic volumes and electron populations reproduced the cell volume V and $F(000)$ within 0.02 and 0.01%, respectively, for both salts, at both experimental and theoretical levels. The integrated Laplacian (L_Ω) gives $L^{err} = (\sum_\Omega L_\Omega^2/N_{atoms})^{1/2}$ within 1.8×10^{-2} e Å^{-2} for both salts, in both experimental and theoretical calculations. Thus, we are confident that the interatomic surfaces were determined with good precision and that the integration results are reliable.

The experimental and theoretical atomic charges for the two salts (Table 5) are in good agreement.

The charge on the K atom is essentially +1 e in both salts. All O atoms show a partial negative charge of about −0.7 e and the total charge of the MnO_4^- and ClO_4^- anions is about −1 e. As expected, the charges on Mn and Cl atoms are lower than the formal oxidation state of +7, and are nearer to +2 e. An electron spectroscopy experiment on potassium permanganate (Reinert *et al.*, 1995) gave the same result, while lower charges (+1.0 − +1.2 for Mn and −0.51 − −0.56 for O atoms)

Figure 4
Bond degree [BD = $H(\mathbf{r}_c)/\rho(\mathbf{r}_c)$, where the units of H are kJ mol^{-1} per atomic unit volume] parameter as a function of $|V(\mathbf{r}_c)|/G(\mathbf{r}_c)$. Triangles and squares refer to experimental and theoretical data, respectively.

Table 5
Net atomic charges (e), calculated by performing an integration over the atomic basins, from the POP refinement (first row) and the DFT calculation (second row).

Atom	$KMnO_4$	$KClO_4$
K	+0.9	+0.7
	+1.0	+1.0
Mn, Cl	+1.6	+2.2
	+1.8	+2.3
O(1)	−0.6	−0.8
	−0.7	−0.8
O(2)	−0.7	−0.7
	−0.7	−0.8
O(3)	−0.6	−0.7
	−0.7	−0.8

Table 6
Averaged distances (Å) of the nuclei from the bond critical points (BCP).

Nucleus–BCP	$KMnO_4$	$KClO_4$
K–BCP	1.47	1.48
O–BCP$_{K-O}$	1.37	1.38
Mn,Cl–BCP	0.85	0.70
O–BCP$_{Mn,Cl-O}$	0.76	0.75

were found in a theoretical study on a free MnO_4^- anion (Nakai *et al.*, 1991).

Tsirelson *et al.* (1998) suggested that 'the distance of the bond critical point from the nucleus can also be considered for an estimation of the ionic radius'. In Table 6, the experimental average nucleus–BCP distances are listed for salts (I) and (II).

The K–BCP, O–BCP$_{K-O}$ and O–BCP$_{Mn-O}$ distances in $KMnO_4$ are very similar to the corresponding ones in $KClO_4$, while the Mn–BCP and Cl–BCP distances are significantly different. The average K–BCP distance (1.47 Å) is near to the ionic radius (1.65 Å) of the K^+ ion with coordination number 8, as reported in the literature (Shannon, 1976). On the contrary, the Mn–BCP distance (0.85 Å) largely differs from the tetrahedral Mn^{7+} ionic radius (0.39 Å) reported in literature, but it is near to the 0.80 Å value of the tetrahedral Mn^{2+} radius (Shannon, 1976). This result is consistent with the charge of about +2 e found for Mn in permanganate. The average O–BCP distance of K—O bonds is greater than the average O–BCP distance of Mn—O or Cl—O bonds, indicating that the O-atom basins are more extended towards K^+ than towards Mn or Cl atoms. The average O–BCP$_{Mn,Cl-O}$ distance (0.76 Å) agrees with the O-atom covalent radius in the literature (0.77 Å) (Huheey *et al.*, 1993).

All BCPs are roughly at the midpoint of the bond, with those of K—O and Mn—O slightly closer to the O atom and those of Cl—O bonds slightly closer to the Cl atom. These results are observed for both theoretical and experimental BCPs.

4. Conclusions

The experimental (120 K) and theoretical (DFT level) electron-density distributions of $KMnO_4$ and $KClO_4$ have been accurately determined in the solid state. The bond classification of the experimental and theoretical density, on the basis of the $|V(\mathbf{r}_c)|/G(\mathbf{r}_c)$ ratio, shows a good agreement for all interactions. According to this classification, the K—O bonds are considered ionic and they are associated with the pure CS type, the Mn—O bonds correspond to the transit CS type and the Cl—O bonds are classified as pure SS type. In addition, the topology of the EED of $Mn_2(CO)_{10}$ (Bianchi *et al.*, 2000;

Farrugia *et al.*, 2003) places the Mn—Mn and Mn—C$_{CO}$ bonds (Mn with zero oxidation state) in the transit CS region, according to the classification in Bianchi *et al.* (2000). Even if the classification by Espinosa *et al.* (2002) was advanced for a hydrogen-bonded system, our results confirm that its validity is not limited to this kind of interaction.

The VSCC dimension of Mn and O atoms in the $KMnO_4$ and $Mn_2(CO)_{10}$ compounds does not vary, notwithstanding the different oxidation state, coordination number and bond type.

Both experiment and theory indicate atomic charges of about +2 e for Mn and Cl atoms in $KMnO_4$ and $KClO_4$, in close agreement with the results obtained from an electron spectroscopy experiment on $KMnO_4$.

The nucleus–BCP distance as a measure of the ionic radius fits well the data reported in the literature for the K^+ and Mn^{2+} ions.

References

Abramov, Yu. A. (1997). *Acta Cryst.* A**53**, 264–269.

Abramov, Yu. A., Brammer, L., Klooster, W. T. & Bullock, R. M. (1998). *Inorg. Chem.* **37**, 6317–6328.

Abramov, Yu. A., Tsirelson, V. G., Zavodnik, V. E., Ivanov, S. A., Brown, I. D. (1995). *Acta Cryst.* B**51**, 942–951.

Bader, R. F. (1990). *Atoms in Molecules. A Quantum Theory*. New York: Oxford University Press.

Bats, J. W. & Fuess, H. (1982). *Acta Cryst.* B**38**, 2116–2120.

Bianchi, R., Gervasio, G. & Marabello, D. (2000). *Inorg. Chem.* **39**, 2360–2366.

Bianchi, R., Gervasio, G. & Marabello, D. (2001*a*). *Helv. Chim. Acta*, **84**, 722–734.

Bianchi, R., Gervasio, G. & Marabello, D. (2001*b*). *Acta Cryst.* B**57**, 638–645.

Bianchi, R., Gervasio, G. & Marabello, D. (2003). Unpublished results.

Clementi, E. & Roetti, C. (1974). *At. Data Nucl. Data Tables*, **14**, 177–478.

Espinosa, E., Alkorta, I., Elguero, J. & Molins, E. (2002). *J. Chem. Phys.* **117**, 5529–5542.

Espinosa, E., Molins, E. & Lecomte, C. (1998). *Chem. Phys. Lett.* **285**, 170–176.

Farrugia, L. J., Mallinson, P. R. & Stewart, B. (2003). *Acta Cryst.* B**59**, 594–600.

Gatti C. (1999). *TOPOND98 User's Manual*. CNR-ISTM, Milano, Italy.

Gatti, C. & Bianchi, R. (1996). Atti XXVI Congresso Nazionale Associazione Italiana di Cristallografia, Alessandria, Italy, p. 139.

Gervasio, G., Bianchi, R. & Marabello, D. (2004). *Chem. Phys. Lett.* **387**, 481–484.

Gottfried, C. & Schusterius, C. (1932). *Z. Kristallogr.* **84**, 65–73.

Hehre, W. J., Ditchfield, R., Stewart, R. F. & Pople, J. A. (1970). *J. Chem. Phys.* **52**, 2769–75.

Hirshfeld, F. L. (1976). *Acta Cryst* A**32**, 239–242.

Huheey, J. E., Keiter, E. A. & Keiter, R. L. (1993). *Inorganic Chemistry: Principles of the Structure and Reactivity.* New York: Harper Collins College Publishers.

International Tables for Crystallography (1995). Vol. C. Dordrecht: Kluwer Academic Publishers.

Johnson, C. K. & Levy, H. A.(1974). *International Tables for X-ray Crystallography*, Vol. IV, pp. 311–316. Birmingham: Kynoch Press.

Lee, J.-J., Lee, G. H. & Wang, Y. (2002). *Chem. Eur. J.* **8**, 1821–1832.

Macchi, P., Garlaschelli, L., Martinengo, S. & Sironi, A. (1999). *J. Am. Chem. Soc.* **121**, 10428–10429.

Macchi, P., Garlaschelli, L. & Sironi, A. (2002). *J. Am. Chem. Soc.* **124**, 14173–14184.

Macchi, P., Proserpio, D. M. & Sironi, A. (1998). *J. Am. Chem. Soc.* **120**, 13429–13435.

Macchi, P. & Sironi, A. (2003). *Coord. Chem. Rev.* **238–239**, 383–412.

Mani, N. V. (1957). *Proc. Indian Acad. Sci.* **46**, 143–151.

Nakai, H., Ohmori, Y. & Nakatsuji, H. (1991). *J. Chem. Phys.* **95**, 8287–8291.

Palenik, G. J. (1967). *Inorg. Chem.* **6**, 503–507.

Pietro, W. J. & Hehre, W. J. (1983). *J. Comput. Chem.* **4**, 241–251.

Reinert, F., Steiner, P. & Hüfner, S. (1995). *J. Magn. Magn. Mater.* **140–144**, 177–178.

Saunders, V. R., Dovesi, R., Roetti, C., Causà, M., Harrison, N. M., Orlando, R. & Zicovich-Wilson, C. M. (1999). *CRYSTAL98 Users' Manual.* University of Torino, Torino, Italy.

Shannon, R. D. (1976). *Acta Cryst.* A**32**, 751–767.

Sheldrick, G. M. (1998). *SHELXTL, Version 5.* Bruker AXS Inc, Madison, WI, USA.

Stewart, R. F. (1976). *Acta Cryst.* A**32**, 565–572.

Stewart, R. F. & Spackman, M. A. (1983). *VALRAY User's Manual.* Department of Chemistry, Carnegie-Mellon University, Pittsburg, PA, USA.

Tsirelson, V. G. (1999). *Acta Cryst.* A**55** Supplement, Abstract M13-OF-003.

Tsirelson, V. G., Avilov, A. S., Abramov, Yu. A., Belokoneva, E. L., Kitaneh, R. & Feil, D. (1998). *Acta Cryst.* B**54**, 8–17.

Zhurova, A., Ivanov, Y., Zavodnik, V. & Tsirelson, V. G. (2000). *Acta Cryst.* B**56**, 594–600.